A study of turbulent wake dynamics using a novel localized stability analysis

By X. S. Liang † AND M. Wang

This paper briefly presents a unified, localized treatment of hydrodynamic stability relating the stability theory to experimental and numerical results, which are in general highly nonlinear, intermittent, and involve multiple scales in space and time. The localization in time is achieved with the multiscale window transform, a mathematical machinery developed by Liang & Anderson (2004); while the spatial dimension is localized through "transfer-transport separation", which is made precise with the introduction of the concept *perfect transfer*. The theory is applied to investigate the dynamics of cylinder wakes. A remarkable observation is that *rapid amplification in perturbation energy does not necessarily correspond to instability*. In a saturated laminar wake, an absolute instability is identified with two local transfer lobes attached to the cylinder surface. In the turbulent case, the instability is located far away downstream and has distinct patterns. The dynamics is structured on three scale windows, among which the meso-scale window hosts a regularly growing mode. This mode is maintained through a primary instability. Although its energy can be ultimately traced to the base flow, the turbulent or sub-mesoscale motion is sustained through two different mechanisms: The first is directly from the background, and is distributed rather symmetrically as two side lobes along the wake boundary; the second comes from a secondary instability of the regular meso-scale process, appearing mainly as a form of monopole in the center. On all the instability maps, there exist sporadic inverse transfer spots. This inverse transfer or self-laminarization has profound implications for vortex suppression, allowing us to propose a generic strategy to get turbulence under efficient control.

1. Introduction

We introduce a novel localized hydrodynamic stability analysis and show how it can be utilized for turbulence research, particularly, for wake dynamics research. Like any infinite dimensional dynamical process, hydrodynamic instabilities are generally localized in space and time. This is especially apparent in the turbulence context, where processes are usually highly nonlinear and tend to occur intermittently over limited domains with irregularity and mobility. A hydrodynamic stability analysis thus should be able to unravel dynamics on a local basis in order to allow for a faithful representation of nature. The challenge is, however, that the conventional concept of stability is a notion over a system (e.g., Lin 1966; Drazin & Reid 1982), to which every location belongs, and hence it is difficult to localize a dynamically isolated hotspot for such an analysis to be performed. This problem is not new. Specific approximate approaches have been sought in tackling certain problems. An example is the parcel stability analysis, which has been applied to the symmetric instability study (see Holton 1992). Other approaches include those used in the study of absolutely and convectively unstable flows (e.g., Pierrehumbert & Swanson 1995; Huerre & Monkewitz 1990), in the treatment of localized standing

† Address: Harvard University DEAS, Pierce Hall, 29 Oxford St, Cambridge, MA 02138

Rankine-Hugoniot shocks (Chakrabarti 1989), and in the investigation of plasma instability (e.g., Chu *et al.* 1996). These analyses are either linear (e.g., WKB method) or formulated in the Lagrangian sense, and as a result their utility is limited.

Liang *et al.* (2004) developed a novel approach to give this old problem a unified solution. Their generalized hydrodynamic stability analysis is localized, nonlinear, and hence applicable to fluid flows on a generic basis. In the following section, we give a brief introduction to the theory. In particular, we show how the interaction between background and perturbation structures can be computed as a field-like (Eulerian) variable in a real time mode. The theory is then applied to study the wake dynamics involving vortex shedding behind a circular cylinder. We first examine a laminar wake (Sec. 3), investigating how it is evolved and sustained. This is followed by an analysis of a turbulent wake (Sec. 4) to study its distinct physics and draw contrast to the laminar case. In Sec. 5, conclusions are drawn and a strategy for optimal turbulence control is proposed.

2. Multiscale window transform and localized stability analysis

Hydrodynamic stability in the classical Lyapunov formalism is essentially an energetic analysis. That is to say, a system is unstable provided that disturbances grow. Here disturbances are measured by a norm, or energy, over the whole domain under concern. The novelty of our new stability analysis approach is to localize the Lyapunov norm to make it a field-like variable. We need to consider the localization both in time and in space.

2.1. *Time localization - Multiscale window transform*

At the heart of the localized stability analysis is how processes in the context of a function space are organized into some subspaces or scale windows with distinct ranges of time scales, as well as time instants. In a classical framework, multiscale decomposition is at odds with energy localization. In Liang *et al.* (2004), this difficulty is overcome through the development of a machinery, multiscale window transform (MWT), which we briefly introduce hereafter. For details, see Liang & Anderson (2004).

MWT tailored specifically to stability analysis can be introduced with the aid of a highly localized scaling basis† $\phi(t)$ (Fig. 1a). The basis is obtained through orthonormalization of the cubic spline. Fig.1b shows its periodized counterpart $\phi_n^j(t)$. Given a field $p = p(t)$, $t \in [0,1]$ a scaling reconstruction (e.g., Strang & Nguyen 1997) can be utilized to fulfill an orthogonal (in $L_2[0,1]$) decomposition to obtain a large scale part $p^{\sim 0}$, and an eddy part $p^{\sim 1}$ or more. These parts are further transformed on a space spanned by $\{\phi_n^{j_1}\}_n$, $n = 0, 1, ..., 2^{j_1} - 1$, with 2^{-j_1} the smallest scale that the given dataset resolves. This transform, which involves scale ranges or windows, rather than individual scales as in traditional transforms, is termed "multiscale window transform". Specifically, we have a large-scale window transform and an eddy window transform in a two-window decomposition.

MWT has a property called "marginalization" which allows one to express the energy for a scale window simply as the square of the transform coefficient for that window. Given a time series $p(t)$, we denote the MWT as $\widehat{p}_n^{\sim \varpi}$, where $\varpi = 0, 1, ...$ signify large-scale window, eddy-scale window, and so forth. The marginalization, which we will henceforth write as $\mathcal{M}_n$, is a special operator of summation over time steps n.

† This is a special case. An MWT in a generic sense does not rely on the choice of basis. This is one aspect where MWT differs from other localized analysis such as wavelet transform.

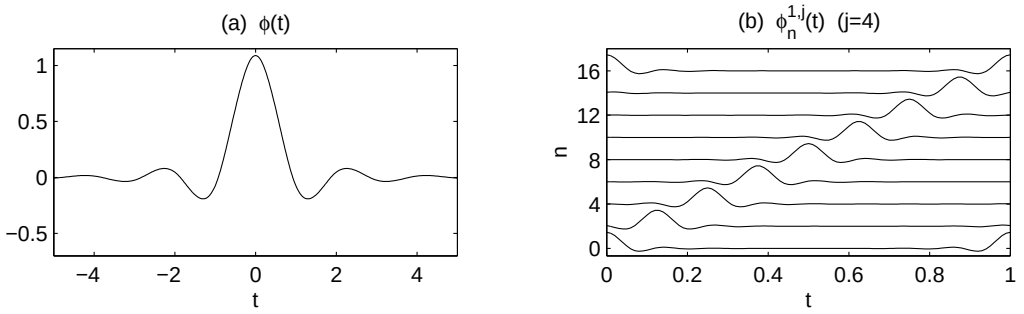

FIGURE 1. (a) Scaling function ϕ constructed via orthonormalization from cubic splines (see Strang & Nguyen 1997). (b) The periodized basis $\phi_n^j(t) = \sum_{\ell=-\infty}^{+\infty} \phi\left(2^j(t+\ell) - n\right)$.

2.2. *Space localization - Transfer-transport separation*

The spatial dimension localization is another crucial issue. In a local sense, perturbation amplification does not necessarily correspond to instability, as energy needed to fuel the growth could be transported from other places into the domain. Liang *et al.* (2004) termed this issue as "transfer-transport separation". In the following, we briefly present their approach to this problem.

Consider an ideal and incompressible fluid flow. The governing equation is

$$\frac{\partial \underline{\mathbf{v}}}{\partial t} = -\nabla \cdot (\underline{\mathbf{v}}\underline{\mathbf{v}}) - \frac{1}{\rho}\nabla P. \tag{2.1}$$

Take an MWT for time step n and window ϖ on both sides and dot with $\widehat{\underline{\mathbf{v}}}_n^{\sim\varpi}$. It gives

$$\dot{K}_n^{\varpi} = NL_n^{\varpi} + Q_{P,n}^{\varpi}, \tag{2.2}$$

where $\dot{K}_n^{\varpi} \approx \frac{1}{2}\widehat{\underline{\mathbf{v}}}_n^{\sim\varpi} \cdot \widehat{\underline{\mathbf{v}}}_n^{\sim\varpi}$, $Q_{P,n}^{\varpi} = -\frac{1}{\rho}\nabla \cdot (\widehat{\underline{\mathbf{v}}}_n^{\sim\varpi} \widehat{P}_n^{\sim\varpi})$, and the nonlinear term $NL_n^{\varpi} = -\left[\nabla \cdot \widehat{(\underline{\mathbf{v}}\underline{\mathbf{v}})}_n^{\sim\varpi}\right] \cdot \widehat{\underline{\mathbf{v}}}_n^{\sim\varpi}$ is a representation of processes intertwined with transport $Q_{K,n}^{\varpi}$ and transfer T_n^{ϖ}. The major issue of spatial localization is how to have these processes precisely separated. This is achieved with the introduction of a concept *perfect transfer*. By definition a perfect transfer T_n^{ϖ} is a process which mediates among scale windows such that $\mathcal{M}_n \sum_{\varpi} T_n^{\varpi} = 0$, i.e., a redistribution of energy among scale windows which does not generate nor destroy energy as a whole. Liang *et al.* (2004) established that NL_n^{ϖ} can be precisely decomposed into a transport and a perfect transfer, and the decomposition is unique. In the incompressible 2-D flow case,

$$T_n^{\varpi} = -\frac{1}{2}\left\{(\widehat{u}_n^{\sim\varpi})^2 \nabla \cdot \underline{\mathbf{v}}_u + (\widehat{v}_n^{\sim\varpi})^2 \nabla \cdot \underline{\mathbf{v}}_v\right\}, \tag{2.3}$$

where $\underline{\mathbf{v}}_S = \frac{\widehat{(\mathbf{v}S)}_n^{\sim\varpi}}{\widehat{S}_n^{\sim\varpi}}$, for $S = u$, and v. For 3-D flow, the third dimension can be added likewise.

Liang *et al.* (2004) showed that, with the aid of T_n^{ϖ}, it is possible to introduce a metric to measure the localized stability. Specifically, they showed that, except for an opposite sign, $CR = (T_n^{\varpi})^{(\varpi+1)\to\varpi}$ followed by a horizontal filtering is in compliance with Lyapunov's norm for a system losing stability from window ϖ to window $\varpi+1$. Here the superscript $(\varpi+1) \to \varpi$ means an interaction analysis that selects out the transfer from window $\varpi+1$ to window ϖ from the nonlinearly intertwined processes. When $CR < 0$,

the flow system is locally unstable, and vice versa. Note *CR* is a field-like variable, and is hence capable of handling any highly localized analysis. For more realistic flows, *CR* may be modified accordingly to ensure consistency with Lyapunov's formalism. But as this nonlinear transfer has essentially captured the dynamics, we might just define it this way.

Note hydrodynamic stability may be understood with $(T_n^{\varpi+1})^{\varpi\to(\varpi+1)}$, as well as from $(T_n^{\varpi})^{(\varpi+1)\to\varpi}$, depending on what a time scale one chooses to observe the problem. They are identical when marginalized, except for the opposite sign. In this case, a system is unstable if $CR > 0$ and vice versa.

Also worthwhile to note is the concept of Reynolds stress.† Conventionally Reynolds stress has been understood as the transfer mechanism between scale windows. Liang *et al.* (2004) established that it does not conserve energy, and as a result, it is problematic in representing transfer processes.

We close this section by remarking that many problems in fluid dynamics are made easy in our framework. In $CR = (T_n^{\varpi})^{(\varpi+1)\to\varpi}$, by switching ϖ from 0 to 1 one may accordingly introduce the concepts of primary instability and secondary instability. Another good example is about convective and absolute instabilities (e.g., Pierrehumbert & Swanson 1995; Huerre & Monkewitz 1990; Oertel 1990 and references therein): A moving negative *CR* means convective instability, while a persisting negative *CR* center implies absolute instability. Likewise, local/global instability can also be studied simply by examining the variation of the influential range of *CR*.

3. Wakes behind a circular cylinder: The laminar case

In this section, we investigate a laminar wake behind a circular cylinder. We particularly want to explore the aspect of the dynamics that sustains the Karman vortex street, through the convenience of the "stability structure" brought forth by our analysis.

3.1. *Model description*

We utilize a numerical model to generate the necessary dataset. The model solves the incompressible Navier-Stokes equations on a C-type mesh using an energy-conserving, hybrid finite-difference/spectral code described in Mittal and Moin (1997). The numerical scheme employs second-order central differences in the streamwise and cross-stream directions, and Fourier collocation in the spanwise direction. The time advancement is of the fractional step type in combination with the Crank-Nicholson method for viscous terms and third order Runge-Kutta scheme for the convective terms. The Poisson equation for pressure is solved using a multigrid iterative procedure at each Runge-Kutta substep.

Dimensionless variables are used in the following analysis, with the cylinder diameter d as the length scale, free-stream velocity U_∞ as the velocity scale, and d/U_∞ as the time scale. We use x, y, and z to denote the streamwise, cross-stream, and spanwise coordinates, respectively, with x and y origins located at the cylinder center.

The laminar flow simulation (2-D) is performed at Re = 200 on a 513×129 mesh, covering a computation domain $-40 \le x \le 25$; $-50 \le y \le 50$. The simulation is initiated with an "impulsive start", and is run until a quasi-steady state is achieved. The results

† Our formalism is equivalent to the classical Reynolds formalism when $j_0 = 0$ and a periodical extension is adopted (see Liang *et al.* 2004).

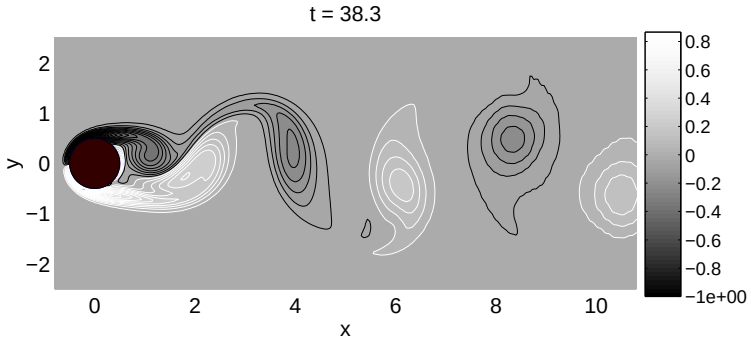

FIGURE 2. A snapshot of the simulated vorticity in a cylinder wake (Re = 200.

are then uniformly mapped onto a cartesian coordinate with $\Delta x = \Delta y = 0.04$, and time stepsize $\Delta t = 0.152$. Shown in Fig. 2 is a snapshot of the simulated vorticity field.

3.2. *Stability structure*

We now investigate the localized stability. It is analyzed from the standing point of energy loss to eddy structures from the large-scale window (that is to say, we analyze it on window 0). This helps us to grasp the stability from a longer time span, without paying too much attention to short scale details. We present only the results after the system reaches an equilibrium, since the transient period is artificial and highly dependent on initial conditions. In this case, a consistent choice of large-scale window bound is $j_0 = 0$. (We have proved in Liang *et al.* (2004) that when $j_0 = 0$ the large-scale window reconstruction is equivalent to the duration average.)

The stability metric in terms of energy loss from the base flow to the eddy window is thereby computed. The result is nearly invariant to time for all the time steps considered because the wake flow is quasi-steady. As shown in Fig. 3 for $t = 38.3$, two negative centers sit symmetrically about the axis $y = 0$. These centers, which embrace the near wake and characterize the energy transfers from the basic flow toward the eddy window, show clearly that the system is absolutely unstable, and the instability is mainly limited within the two negative lobes attached to the cylinder. An analysis using the initial evolution data (not shown here) exhibits how this absolute instability is invoked.

Also shown in Fig. 3a is that CR is non-positive everywhere throughout the domain. That is to say, a global instability has been excited. In contrast to the classical notion, the global instability does not just mean a uniform energy transfer everywhere. Rather, it has a spatial structure.

It is conventional to read instability by examining perturbation growth from simulations. Here we also plot the perturbation/eddy energy growth $\dot{K}^{eddy}$. Shown in Fig. 3b is the $\dot{K}^{eddy}$ for the same time instant as in Fig. 3a. Apparently, the distributions in these two maps are different. Eddy energy grows very fast along $y = 0$ in the near wake, while in the same region the transfer is virtually zero. It can be misleading to assess the stability of a flow system by visual inspection of the simulated fields.

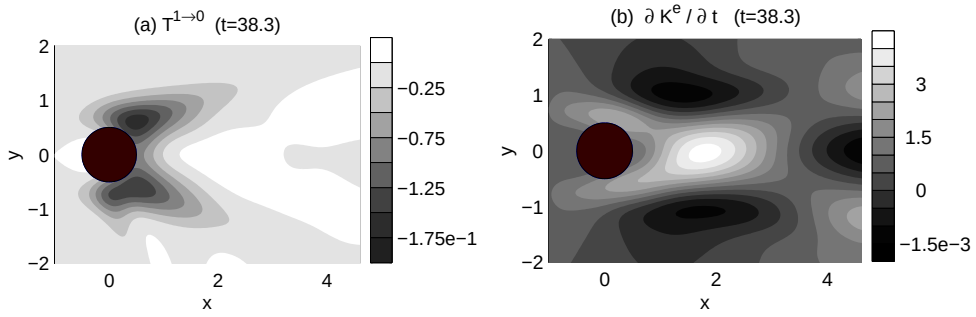

FIGURE 3. (a) Instability metric for $t = 38.3$ in terms of energy loss from the large-scale window to the eddy window. Negative transfer indicates instability. (b) Time rate of change of eddy energy $\dot{K}^{eddy}$ for $t = 38.3$). Positive $\dot{K}^{eddy}$ means gain in eddy energy.

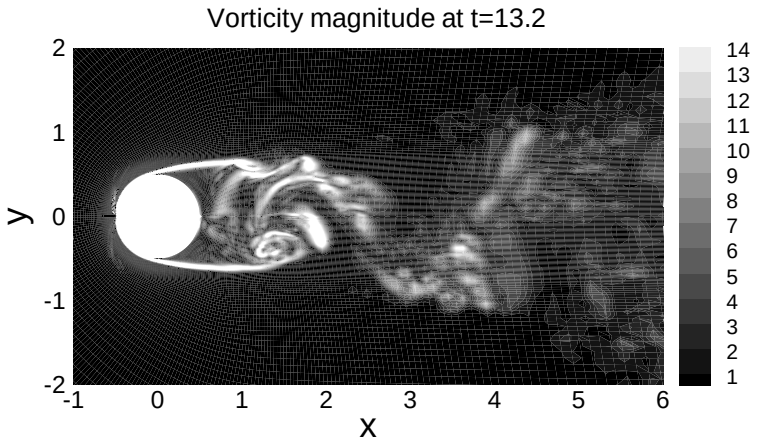

FIGURE 4. A snapshot of the instantaneous vorticity magnitude for the turbulent wake. The Reynolds number is 3900.

4. Wakes behind a circular cylinder: The turbulent case

4.1. *Model description*

To generate a turbulent dataset at Re=3900, we adopt the same numerical model as in the preceding section except that the Navier-Stokes equations are solved in conjunction with the dynamic subgrid scale model (Germano *et al.* 1991; Lilly 1992). In the simulation, $401 \times 120 \times 48$ grid points are used, and the domain size is given by $-22 \leq x \leq 17$, $-24 \leq y \leq 24$, and $-\pi/2 \leq z \leq \pi/2$. The computational solutions have been validated against previous results in terms of key parameters such as the drag coefficient and vortex-shedding frequency (Strouhal number). After the computation reaches a statistical equilibrium, we interpolate the results onto a uniform cartesian mesh ($\Delta x = 0.04, \Delta y = 0.02, \Delta z = \pi/48$) and $2^8 = 256$ equal time steps with $\Delta t = 0.0387$. Fig. 4 shows the instantaneous vorticity magnitude in a spanwise section at $t = 13.2$ (arbitrary starting time).

4.2. *Window bound determination*

Turbulence problems involve more complicated scale window structures. Before moving on to stability analysis, we need to determine the respective scale window bounds. We

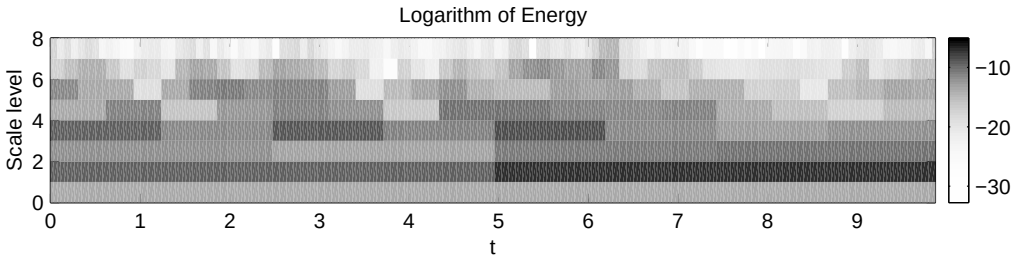

FIGURE 5. Time wavelet spectrum analysis for u at point $(2, -0.5, 0)$. Unfolded on the map is the logarithm of the square of wavelet transform coefficients. The abscissa is time, and the ordinate scale level j, which is defined such that $2^{-j}T$ (T = time duration) is the time scale.

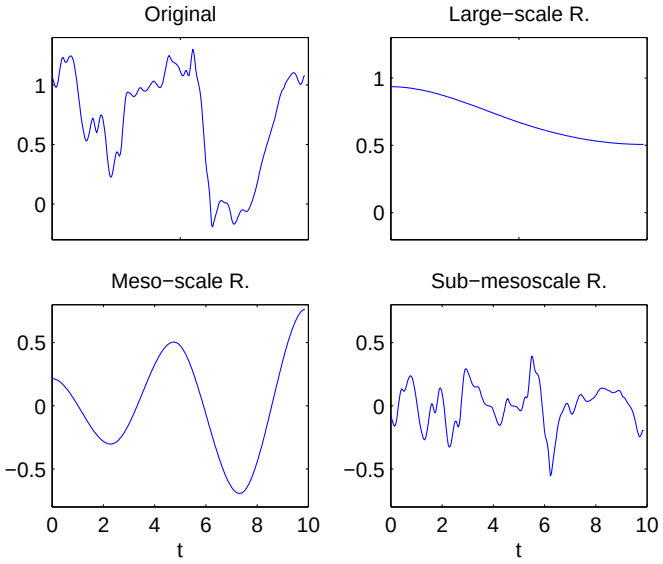

FIGURE 6. Reconstructions of the time series of u in Fig. 5. Parameters used are $j_0 = 1$, and $j_1 = 2$.

use a wavelet time spectrum analysis for this purpose. The time series are chosen from the velocity components at several typical points within the wake.

We only present the analysis of one time series. Fig. 5 displays the spectrum for u at point $(2, -0.5, 0)$. For clarity, the time average has been removed from the signal. We see from the figure that there is a clear peak at scale level $j = 1$, and another one between $j = 3$ and 4. This implies that the choice $j_0 = 0$ and $j_1 = 2$ allows for a demarcation of the function space into a well-defined large-scale window, a meso-scale window, and a sub-mesoscale window. The reconstructions with these parameters (Fig. 6) present from another point of view this partition. The growing oscillating meso-scale reconstruction hosts the time scale of vortex shedding, which is modulated by the slower varying large-scale reconstruction. The sub-mesoscale window represents the rapidly varying small scale turbulence. We are to investigate how the meso-scale window arises, and where the turbulent sub-mesoscale structure derives its energy.

4.3. *Turbulence structure analysis*

As in the laminar case, we continue to analyze the hydrodynamic stability from a longer-time span point of view. That is to say, we use energy loss from one window to another, rather than energy gain within a window, as the criterion. The results are presented in a spanwise plane, although the analysis is fully three-dimensional. The turbulent flow field is statistically equivalent in all the spanwise planes, but over the time period considered, the stability metric is not invariant to the spanwise location.

Figure 7 shows how energy is transferred from the background to the meso-scale structure. Here negative value indicates instability. There are two centers of instability for all the time steps shown. From the sequence, two evolutionary patterns are evident. The first is the orientation evolution: In the beginning the two centers are aligned in a northwest-southeast pattern; their relative location varies gradually into a juxtaposition symmetric around $y = 0$, and finally they evolve into a southwest-northeast orientation. The second is the relative transfer strength between these two centers. Originally, the southern center is much weaker than the northern one, but beginning at $t = 4.1$, they switch status, and by $t = 8.8$, a pattern opposite to the original appears.

In comparison to Fig. 7, the energy lost from the background to the turbulent structures are fairly symmetric about the x-axis (see Fig. 8). This is to some degree similar to the laminar case, although the transfer strength oscillates, and the hotspots are detached from the cylinder.

The above computations are based on the large-scale window. Interactions between the meso-scale and sub-mesoscale processes also require analysis for the meso-scale window. Shown in Fig. 9 is the energy loss from the meso-scale process to the turbulent processes. In contrast to the dipole structure in Figs. 7 and 8, here the transfer is mainly within a monopole except in the beginning. And, moreover, the monopole lies near the x-axis. The energy gained by the meso-scale process from the basic flow then cannot be used directly to fuel the turbulence. It must be first transported from the two lobes to the center before the transfer occurs.

The above observations suggest that there is clearly a primary instability, followed by a secondary instability, in the turbulent wake. The primary instability is composed of two parts: one accounts for the meso-scale growing mode; another for the turbulence along the wake boundary. The meso-scale dynamics is regular, as is shown in Fig. 6. The wake becomes asymmetric about the x-axis because this process is excited in an asymmetric way. The secondary instability occurs mainly in the middle near the x-axis. It funnels energy to sustain the turbulence there. Both the turbulent motions along the wake boundary and in the middle acquire energy in a fairly symmetric way, indicating that the system is in a statistical equilibrium.

A remarkable feature in the transfer maps in Figs. 7, 8 and 9 is the positive spots/centers sandwiched in the instability structures. These inverse transfers indicate that, even though the flow is turbulent, there exist processes which introduce orders rather than chaos to the system. We will see later in the discussion that these inverse transfers may have profound implications for turbulence control.

5. Discussion and conclusions

We have briefly introduced a localized hydrodynamic stability analysis to relate stability theory to experimental and numerical data, which are in general highly nonlinear

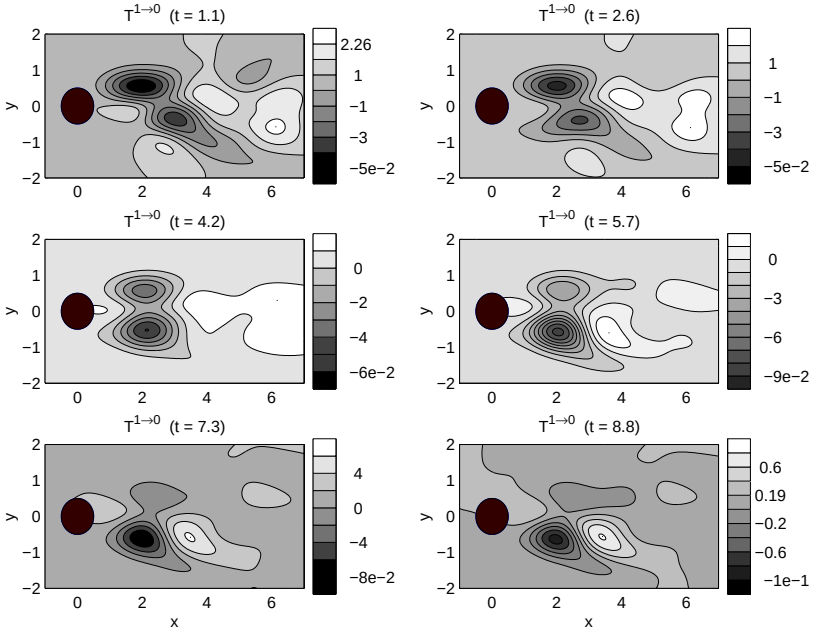

FIGURE 7. Stability metric *CR* in terms of energy transfer from the large-scale window to the meso-scale window for the turbulent wake. Negative values indicate instability.

and intermittent in space and time. We have utilized the theory to investigate the wake behind a cylinder, both in a laminar flow and in a turbulent flow.

The localized stability analysis is developed on a subspace decomposition-based and localized mathematical machinery, multi-scale window transform. In this analysis, a flow system is organized into some appropriately defined time scale windows. The classical formalism in the sense of Lyapunov is then localized in time to obtain a metric to measure the hydrodynamic instability. The key to spatial localization is the transfer-transport separation, which is made possible through introducing the concept of *perfect transfer*. For a fluid flow, the resulting criterion of instability bears a spatio-temporal structure, which is conceptually different from the classical formalism where stability is a notion over the whole system. This allows for much more flexibility in investigating flows with regions of interest that are difficult to demarcate. It is particularly useful for open flows, and flows with dynamics mobile in nature, such as those involving convective instability and absolute instability.

The theory has been applied to investigate the wake dynamics behind a circular cylinder. We have examined two different cases: a laminar wake (Re=200), and a turbulent wake (Re=3900). In the laminar case, the metric shows a symmetric transfer pattern, with two lobes of local absolute instability attached to the cylinder surface. A global instability mode is also seen at the stage. In contrast to the classical formalism, the eddy energy growth pattern does not necessarily imply instability.

The turbulent wake case shows a more complicated and interesting instability structure. Processes involved are structured on three distinct scale windows, among which the meso-scale flow sees a clear regularly growing mode for the time period analyzed. A primary instability is identified, with transfer centers appearing in pair along the wake boundary. It provides energy both for the meso-scale window and for the sub-mesoscale

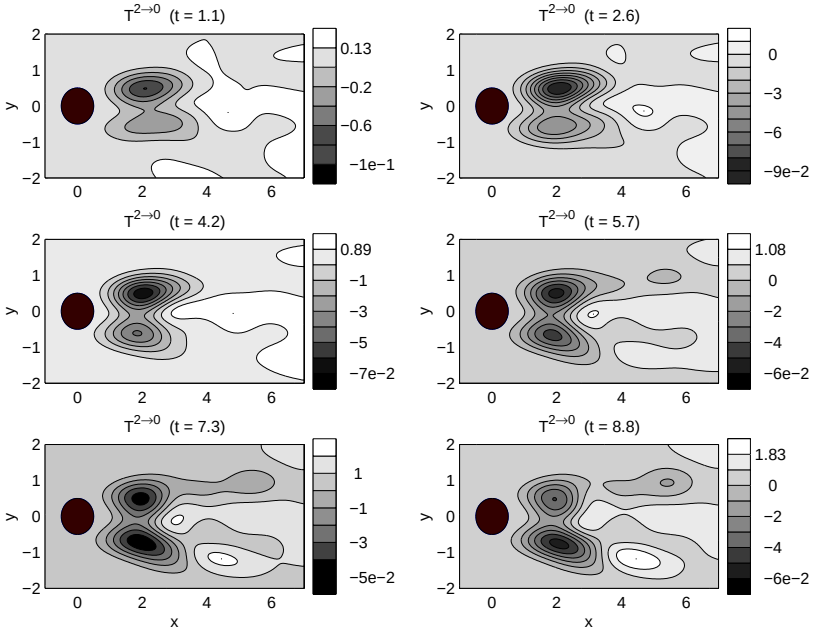

FIGURE 8. Stability metric $\mathcal{CR}$ in terms of energy transfer from the large-scale window to the sub-mesoscale window for the turbulent wake. Negative values indicate instability.

turbulence window. The transfer-center pair for the meso-scale window oscillates in orientation as well as strength, accounting mostly for the asymmetry of the wake vortex shedding, while that for the sub-mesoscale window adopts a pattern fairly symmetric in location around the x-axis. The turbulence also derives its energy from the meso-scale window. This secondary instability is in a monopole form and appears mainly in the center around the x-axis. Both the primary instability and the secondary instability are absolute in character.

A potential application of the above research is flow control. Based on previous studies (e.g., Huerre & Monkewitz 1990), absolute instability plays a pivotal role in vortex shedding, and as a result, a crucial step in suppressing the formation of the Karman vortex street is to identify the absolute instability regions. Our methodology provides a natural and easy way to achieve this. Although there is still some distance to go before a mature scheme of vortex suppression is formulated, it seems reasonable to suggest that control should be best applied at the maximum energy transfer centers or at locations directly upstream of these centers. In the laminar case the instability lobes are attached to the cylinder surface and their centers are downstream of the top and bottom of the cylinder, suggesting that applying control near these locations may be effective. Indeed, our simple numerical experiments using surface suction show that the areas between 70 to 90 degrees and between -70 to -90 degrees from the x-axis are the most effective suction locations for suppressing vortex shedding and reducing drag on the cylinder. Controls in areas below 50 degrees and above -50 degrees are counterproductive. We will explore this in a more systematic fashion in the future.

We have seen that on all the instability patterns there are sandwiched stable centers. These stable structures indicate that, although the flow is turbulent, processes of inverse transfer or self-laminarization may exist. This phenomenon has profound implications.

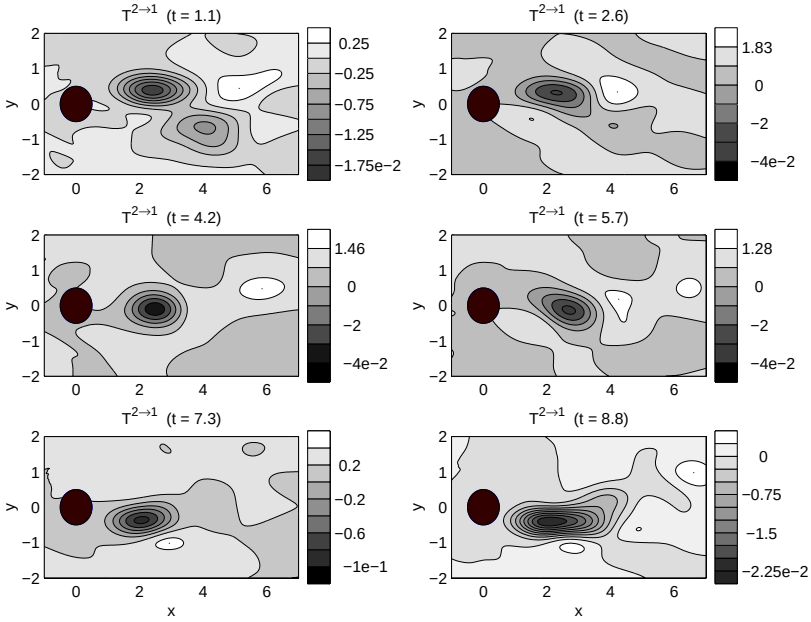

FIGURE 9. Stability metric CR in terms of energy transfer from the meso-scale window to the sub-mesoscale window for the turbulent wake. Negative values indicate instability.

As is well known, the objective of turbulence control is to inhibit eddy energy from being generated, and accordingly, the traditional control strategy is based on suppression of turbulence growth. The problem is, *looking solely at the turbulence growth could be misleading, as energy increase does not necessarily occur in accordance with transfer* (cf. Fig. 3). In a region with eddy energy growing the transfer could be toward the large-scale flow. This is best illustrated in the two-point system in Fig. 10, where eddy energy (K_1^{eddy} and K_2^{eddy}) grows at both locations 1 and 2, while the transfer at location 2 is toward the large-scale window. Control of the perturbation energy growth at both points 1 and 2 indeed helps to suppress the onset of turbulence, but it is not optimal in terms of energy savings. At point 2, there is an intrinsic trend of laminarization. Suppression of K_2^{eddy} defeats this trend as well, and therefore reduces the control performance. To take advantage of this laminarization, the control should be applied at point 1 only, and the optimal objective functional should be chosen to be T_1, rather than $K_1^{eddy} + K_2^{eddy}$.

REFERENCES

CHAKRABARTI, S. K. 1989 Standing Rankine-Hugoniot shocks in the hybrid model flows of the black hole accretion and winds. *Astrophys. J.* **347 (1)**, 365-372.

CHU, M. S., GREENE, J. M., LAO, L. L., MILLER, R. L., BONDESON, A., SAUTER, O., RICE, B. W., STRAIT, E. J., TAYLOR, T. S., & TURNBULL, A. D. 1996 Resistive interchange modes in negative central shear tokamaks with peaked pressure profiles. *Phys. Rev. Lett.* **77(13)**, 2710-13.

DRAZIN, P.G., & REID, W. H. 1982: *Hydrodynamic Stability.* Cambridge University Press. Cambridge, UK.

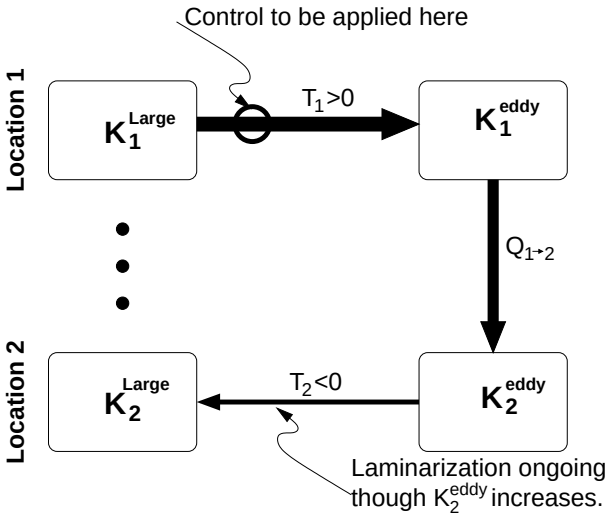

FIGURE 10. Schematic of the eddy energy transport and transfer for a two-point turbulent system. T and Q signify transfer and transport, respectively. An arrow indicates the direction of an energy flow, with its thickness standing for strength. In this case, transfer is toward the large scale at point 2, but K_2^{eddy} still grows because of the transport (advection) of K_1^{eddy} from point 1. For optimal results, control should be placed at location 1 only.

GERMANO, M., PIOMELLI, U., MOIN, P., & CABOT, W. H. 1991 A dynamic subgrid-scale eddy viscosity model. *Phys. Fluids A* **3**, 1760–1765.

HOLTON, J. R. 1992 *An Introduction to Dynamic Meteorology.* Academic Press. San Diego, California.

HUERRE, P. & MONKEWITZ, P. 1990 Local and global instabilities in spatially developing flows. *Annu. Rev. Fluid Mech.* **22**, 473-537.

LIN, C. C. 1966 *The Theory of Hydrodynamic Stability.* Cambridge U Press. Cambridge, UK.

LIANG, X. S. & ANDERSON D. G. M 2004 Multiscale window transform. (in preparation).

LIANG, X. S., STONE, H. A., ANDERSON, D. G. M., & WANG, M. 2004 A unified localized hydrodynamic instability analysis for incompressible fluid flows. (in preparation).

LILLY, D. K. 1992 A proposed modification of the Germano subgrid scale closure method. *Phys. Fluids A* **4**, 633–635.

MITTAL, R.& MOIN, P. 1997 Suitability of upwind-biased finite difference schemes for large-eddy simulation of turbulence flows. *AIAA J.* **35**, 1415–1417.

OERTEL, H., JR. 1990 Wakes behind blunt bodies. *Annu. Rev. Fluid Mech.* **22**, 539-559.

PIERREHUMBERT, R. T., & SWANSON, K. L. 1995 Baroclinic Instability. *Ann. Rev. Fluid Mech.* **27**, 419-467.

STRANG, G. & NGUYEN, T. 1997 *Wavelets and Filter Banks.* Wellesley-Cambridge Press. Wellesley, MA.